# Weakly nonlinear analysis of Rayleigh-Bénard convection in a non-Newtonian fluid between plates of finite conductivity: Influence of shear-thinning effects

Mondher Bouteraa and Chérif Nouar*
*LEMTA UMR 7563 CNRS, Université de Lorraine ENSEM, 2 Avenue de la Forêt de Haye, TSA 60604-54516 Vandoeuvre lès Nancy cedex, France*
(Received 21 July 2015; published 17 December 2015)

Finite-amplitude thermal convection in a shear-thinning fluid layer between two horizontal plates of finite thermal conductivity is considered. Weakly nonlinear analysis is adopted as a first approach to investigate nonlinear effects. The rheological behavior of the fluid is described by the Carreau model. As a first step, the critical conditions for the onset of convection are computed as a function of the ratio $\xi$ of the thermal conductivity of the plates to the thermal conductivity of the fluid. In agreement with the literature, the critical Rayleigh number $\mathrm{Ra}_c$ and the critical wave number $k_c$ decrease from 1708 to 720 and from 3.11 to 0, when $\xi$ decreases from infinity to zero. In the second step, the critical value $\alpha_c$ of the shear-thinning degree above which the bifurcation becomes subcritical is determined. It is shown that $\alpha_c$ increases with decreasing $\xi$. The stability of rolls and squares is then investigated as a function of $\xi$ and the rheological parameters. The limit value $\xi_c$, below which squares are stable, decreases with increasing shear-thinning effects. This is related to the fact that shear-thinning effects increase the nonlinear interactions between sets of rolls that constitute the square patterns [M. Bouteraa *et al.*, J. Fluid Mech. **767**, 696 (2015)]. For a significant deviation from the critical conditions, nonlinear convection terms and nonlinear viscous terms become stronger, leading to a further diminution of $\xi_c$. The dependency of the heat transfer on $\xi$ and the rheological parameters is reported. It is consistent with the maximum heat transfer principle. Finally, the flow structure and the viscosity field are represented for weakly and highly conducting plates.

DOI: 10.1103/PhysRevE.92.063017 PACS number(s): 47.20.Bp, 47.50.Gj

## I. INTRODUCTION

Recently, a weakly nonlinear stability analysis of thermal convection in a layer of a non-Newtonian fluid between two horizontal plates, of infinite thermal conductivity, heated from below was considered by Bouteraa *et al.* [1]. Assuming the fluid purely viscous and shear thinning, they studied the influence of shear-thinning effects on the nature of the primary bifurcation and the pattern selection. The possibility of wall slip was taken into account by using Navier's slip law at top and bottom walls. It was shown that the bifurcation is supercritical for moderately shear-thinning effects and becomes subcritical for strongly shear-thinning effects. The critical value of the degree of shear-thinning $\alpha_c$ defined by Eq. (14), above which the bifurcation becomes subcritical is determined as a function of a dimensionless slip length parameter. It is demonstrated that near the threshold of the convection, only rolls are stable and this stability is reinforced by the shear-thinning behavior.

In experimental situations, however, the thermal conductivity of the plates is finite. Furthermore, in some situations, the plates are much poorer conductors than the fluid. For instance, in LeGal and Croquette [2], the plates are made of Plexiglas and the fluid is water. The ratio $\xi$ of the thermal conductivity of the plates $\hat{k}_p$ to the thermal conductivity of the fluid $\hat{k}$ is $\xi = 0.4$. In Gorius *et al.* [3], a layer of mercury is bounded by two plates made of a resin, with a ratio $\xi = 0.23$. In Kebiche [4] and Kebiche *et al.* [5], the horizontal plates are made of polycarbonate and the fluid is an aqueous solution of carboxymethyl cellulose or carbopol; the ratio $\xi$ is estimated to $\xi = 0.25$. In these situations, as well as those encountered in some engineering convection problems and in geophysics, the assumption that the plates are held at fixed and uniform temperatures loses its validity. The boundary conditions that have to be satisfied are continuity of temperature and heat flux at the interface between the fluid and the plate.

For a Newtonian fluid, the effect of imperfect conducting plates on the Rayleigh-Bénard convection was investigated by several authors. First, in the linear theory frame, Sparrow *et al.* [6] and Hurle *et al.* [7] (see also Riahi [8], Clever and Busse [9], and Holmedal *et al.* [10] for plates of arbitrary thicknesses and conductivities) showed that the critical Rayleigh number $\mathrm{Ra}_c$ and the critical wave number $k_c$, vary continuously from 1708 to 720 and from 3.11 to 0, when the ratio of thermal conductivities decreases from infinity to zero. According to Cerisier *et al.* [11] a temperature fluctuation occurring in the liquid close to a nearly insulating plate persists and distorts the temperature distribution. This temperature distortion can lead to an instability of the fluid layer. As a consequence, the temperature gradient is small and the fluid organizes in a pattern with a small wave number.

Exploiting the fact that for nearly insulating walls ($\xi \ll 1$) the horizontal scale of convection is much larger than the depth of the fluid, Busse and Riahi [12] considered weakly nonlinear three-dimensional solutions in the case of infinitely thick plates. They showed that near the onset, square convection cells are the stable planform, in contrast with two-dimensional rolls which are the only stable convection pattern in a symmetrical situation with isothermal boundary conditions. This result was confirmed and extended to fully nonlinear convection, with plates of finite thickness, by Proctor [13] using a "shallow water theory" adapted for the Rayleigh-Bénard convection by Chapman and Proctor [14]. Afterwards, Jenkins and Proctor [15] considered three-dimensional finite-amplitude thermal

*cherif.nouar@univ-lorraine.fr

 

convection with finite thickness and finite thermal conductivity of the bounding plates. They determined the critical value $\xi_c$ of the thermal conductivities ratio at which the preferred planform changes from square cell ($\xi < \xi_c$) to roll ($\xi > \xi_c$) as function of the Prandlt number. When the thickness of the plates is of the same order as that of the fluid layer and for $\mathrm{Pr} \geqslant 10$, rolls should be observed when $\xi > 1$ and squares when $\xi < 1$. This is in agreement with LeGal and Croquette's experiments [2]. For low Prandtl number, say, $\mathrm{Pr} \leqslant 0.1$, Jenkins and Proctor [15] found that $\xi_c \propto \mathrm{Pr}^4$.

The objective of the present paper is twofold: first, to study the influence of shear-thinning effects on $\xi_c$ and, second, to determine the nature of the primary bifurcation depending on the shear-thinning degree and the ratio of thermal conductivities. We hope that our findings will shed new light on the interpretation of the results obtained by Kebiche [4] and Kebiche *et al.* [5], although the fluid used in Ref. [5] is not only shear thinning but has also a yield stress.

The paper is organized as follows. In Sec. II, the mathematical formulation of the problem is presented. In Sec. III, the linear stability analysis for the onset of convective flow is reinvestigated. The critical Rayleigh number ($\mathrm{Ra}_c$) and wave number ($k_c$) are determined as a function of $\xi$. Section IV presents briefly the procedure used in the weakly nonlinear stability analysis. The results are discussed in Sec. V. The critical value of the shear-thinning degree above which the bifurcation becomes subcritical is determined as a function of $\xi$. The pattern selection near the threshold of convection is investigated in terms of $\alpha$ and $\xi$. For a significant deviation from the critical conditions, higher-order solutions are computed in Sec. VI. Section VII provides information on the flow structure and the heat transfer. A concluding discussion is given in the last section of the paper.

## II. PROBLEM FORMULATION

### A. General equations and parameters

We consider a layer of shear-thinning fluid of depth $\hat{d}$ confined between two horizontal plates that are infinite in extent and which have a thickness $\Lambda\hat{d}$, where $\Lambda$ is of order unity. The outer surface of the bottom and top plates are kept at constant temperatures, respectively $\hat{T}_0 + \Delta\hat{T}/2$ and $\hat{T}_0 - \Delta\hat{T}/2$, with $\Delta\hat{T} > 0$. The fluid has density $\hat{\rho}$, thermal conductivity $\hat{k}$, thermal coefficient expansion (at constant pressure) $\hat{\beta}$, and viscosity $\hat{\mu}_0$ at zero shear rate. The thermal conductivity of the slabs is $\hat{k}_p$. Because of the thermal expansion, the temperature difference between the two plates induces a vertical density stratification. Heavy cold fluid is above a light warm fluid. For small $\Delta\hat{T}$, the fluid remains at rest and the heat is transferred by conduction. In the fluid, $0 < \hat{z} < \hat{d}$, the hydrostatic solution and the temperature profile are

$$\frac{d\hat{P}}{d\hat{z}} = -\hat{\rho}_0\hat{g}[1 - \hat{\beta}(\hat{T} - \hat{T}_0)] \quad \text{and}$$
$$\hat{T}_{\mathrm{cond}} = \hat{T}_0 + \frac{\Delta\hat{T}}{1 + 2\Lambda/\xi}\left[\frac{1}{2} - \frac{\hat{z}}{\hat{d}}\right], \tag{1}$$

where $\hat{g}$ is the acceleration due to gravity. Here the $z$ axis is directed upwards, with the origin located at the bottom plate. The reference temperature $\hat{T}_0$ is the temperature in the middle of the fluid layer and $\hat{\rho}_0$ is the fluid density at $\hat{T}_0$. The temperature difference between the top and the bottom of the fluid layer is $\Delta\hat{T}_f = \Delta\hat{T}/(1 + 2\Lambda/\xi)$.

The temperature profile in the top and bottom plates are

$$\hat{T}_{\mathrm{cond}} = \hat{T}_0 + \frac{\Delta\hat{T}}{\xi + 2\Lambda}\left[1 - \frac{1}{2}\xi - \frac{\hat{z}}{\hat{d}}\right], \quad \hat{d} \leqslant \hat{z} \leqslant (1 + \Lambda)\hat{d}, \tag{2}$$

and

$$\hat{T}_{\mathrm{cond}} = \hat{T}_0 + \frac{\Delta\hat{T}}{\xi + 2\Lambda}\left[\frac{1}{2}\xi - \frac{\hat{z}}{\hat{d}}\right], \quad -\Lambda\hat{d} \leqslant \hat{z} \leqslant 0. \tag{3}$$

When $\xi$ is low, a large part of $\Delta\hat{T}$ occurs across the plates and remains only a small part $\Delta\hat{T}_f$ of $\Delta\hat{T}$, acting as the driving force for the convection. When $\Delta T_f$ exceeds a critical value, the buoyancy force overcomes the dissipative effects, i.e., viscous and heat diffusion, the convection sets in, and so-called convective patterns emerge. The stability of the hydrostatic solution is considered by introducing temperature and pressure perturbation as well as a fluid motion. The Boussinesq approximation is adopted, i.e., the temperature dependence of the fluid properties can be neglected except for the temperature-induced density difference in the buoyant force that drives the flow. The heat production due to viscosity is neglected. Here and in what follows, the quantities with hat ($\hat{\cdot}$) are dimensional. Distances are scaled with $\hat{d}$; velocity with $\hat{\kappa}/\hat{d}$, where $\hat{\kappa}$ is the thermal diffusivity of the fluid; time with $\hat{d}^2/\hat{\kappa}$ (characteristic time scale of thermal diffusion); temperature with $\Delta\hat{T}_f$; and pressure and stresses with $\hat{\kappa}\hat{\mu}_0/\hat{d}^2$. Using these scales, the dimensionless perturbation equations read:

$$\boldsymbol{\nabla}\cdot\boldsymbol{u} = 0, \tag{4}$$
$$\frac{1}{\mathrm{Pr}}\left[\frac{\partial\boldsymbol{u}}{\partial t} + \boldsymbol{u}\cdot\boldsymbol{\nabla}\boldsymbol{u}\right] = -\boldsymbol{\nabla}p + \mathrm{Ra}\,\theta\,\boldsymbol{e}_z + \boldsymbol{\nabla}\cdot\boldsymbol{\tau}, \tag{5}$$
$$\frac{\partial\theta}{\partial t} + \boldsymbol{u}\cdot\boldsymbol{\nabla}\theta = \boldsymbol{u}\cdot\boldsymbol{e}_z + \boldsymbol{\nabla}^2\theta, \tag{6}$$

in the fluid and

$$\frac{\partial\tilde{\theta}}{\partial t} = \frac{\hat{\kappa}_p}{\hat{\kappa}}\boldsymbol{\nabla}^2\tilde{\theta} \tag{7}$$

in the bounding slabs. Here $\boldsymbol{e}_z$ denotes the unit vector in the vertical direction, $\boldsymbol{u}(\boldsymbol{x},t) = u\boldsymbol{e}_x + v\boldsymbol{e}_y + w\boldsymbol{e}_z$ is the fluid velocity and $p(\boldsymbol{x},t)$ and $\theta(\boldsymbol{x},t)$ represent the pressure and temperature deviations from their values in the conduction state. The temperature perturbation in the slabs is denoted $\tilde{\theta}(\boldsymbol{x},t)$. The position vector $\boldsymbol{x}$ has components $x,y,z$. The Rayleigh number Ra and the Prandtl number Pr are defined by

$$\mathrm{Ra} = \frac{\hat{\rho}_0\hat{g}\hat{\beta}\Delta\hat{T}_f\hat{d}^3}{\hat{\kappa}\,\hat{\mu}_0}; \quad \mathrm{Pr} = \frac{\hat{\mu}_0}{\hat{\rho}_0\,\hat{\kappa}}. \tag{8}$$

### B. Rheological model and parameters

The fluid is assumed to be purely viscous and shear thinning. The viscous stress-tensor

$$\boldsymbol{\tau} = \mu(\Gamma)\dot{\boldsymbol{\gamma}} \quad \text{with} \quad \dot{\boldsymbol{\gamma}} = \boldsymbol{\nabla u} + (\boldsymbol{\nabla u})^T \tag{9}$$

and the rate-of-strain tensor of the second invariant

$$\Gamma = \tfrac{1}{2}\dot{\gamma}_{ij}\dot{\gamma}_{ij}. \tag{10}$$

The Carreau model is given by

$$\frac{\hat{\mu} - \hat{\mu}_\infty}{\hat{\mu}_0 - \hat{\mu}_\infty} = (1 + \hat{\lambda}^2\,\hat{\Gamma})^{\frac{n_c-1}{2}}, \tag{11}$$

with $\hat{\mu}_0$ and $\hat{\mu}_\infty$ the viscosities at low and high shear rate, $n_c < 1$ the shear-thinning index, and $\hat{\lambda}$ the characteristic time of the fluid. The location of the transition from the Newtonian plateau to the shear-thinning regime is determined by $\hat{\lambda}$, since $1/\hat{\lambda}$ defines the characteristic shear rate for the onset of shear thinning. Increasing $\hat{\lambda}$ reduces the Newtonian plateau to lower shear rates. The infinite shear viscosity, $\hat{\mu}_\infty$, is generally associated with a breakdown of the fluid and is frequently significantly smaller ($10^{-3}$ to $10^{-4}$ times smaller) than $\hat{\mu}_0$, see Bird *et al.* [16] and Tanner [17]. The ratio $\hat{\mu}_\infty/\hat{\mu}_0$ will be thus neglected in the following. The dimensionless effective viscosity is then

$$\mu = \frac{\hat{\mu}}{\hat{\mu}_0} = (1 + \lambda^2\,\Gamma)^{\frac{n_c-1}{2}} \quad \text{with} \quad \lambda = \frac{\hat{\lambda}}{\hat{d}^2/\hat{\kappa}}. \tag{12}$$

The Newtonian behavior, $\hat{\mu} = \hat{\mu}_0$, is obtained by setting $n_c = 1$ or $\hat{\lambda} = 0$.

For a small amplitude disturbance, the viscosity can be expanded about the hydrostatic solution,

$$\mu = 1 + \left(\frac{n_c - 1}{2}\right)\lambda^2\,\Gamma + \frac{1}{2}\left(\frac{n_c-1}{2}\right)\left(\frac{n_c-3}{2}\right)\lambda^4\Gamma^2 + \ldots \tag{13}$$

At lowest nonlinear order, a relevant rheological parameter is the "degree of shear thinning,"

$$\alpha = \left|\frac{d\mu}{d\Gamma}\right|_{\Gamma=0} = \frac{1 - n_c}{2}\lambda^2. \tag{14}$$

### C. Boundary conditions

For the perturbation velocity $\boldsymbol{u}$, the conditions imposed on the top and bottom plates are either no-slip (no-slip boundary conditions NSBC), which implies

$$\boldsymbol{u} = 0 \quad \text{at} \quad z = 0,1, \tag{15}$$

or stress-free (stress-free boundary conditions SFBC), which implies

$$\frac{\partial u}{\partial z} = \frac{\partial v}{\partial z} = w = 0 \quad \text{at} \quad z = 0,1. \tag{16}$$

For thermal boundary conditions, a constant and uniform temperature is assumed on the outer surface of each plate

$$\tilde{\theta} = 0 \quad \text{at} \quad z = -\Lambda, 1 + \Lambda. \tag{17}$$

The continuity condition for temperature and heat flux are

$$\theta = \tilde{\theta} \quad \text{at} \quad z = 0,1, \tag{18}$$

$$D\theta = \xi\, D\tilde{\theta} \quad \text{at} \quad z = 0,1, \tag{19}$$

where $D \equiv \frac{\partial}{\partial z}$ and $\xi = \frac{\hat{k}_p}{\hat{k}}$.

### D. Reduction: Elimination of the pressure

In the momentum equations, the pressure field can be eliminated using the curl of Eq. (5). We then take the curl of Eq. (5) one more time. Using the continuity equation, and projecting onto $\boldsymbol{e}_z$, we get the following evolution equations for the vertical vorticity $\zeta$ and the vertical velocity $w$:

$$\frac{\partial \zeta}{\partial t} + \boldsymbol{e}_z \cdot \boldsymbol{\nabla} \times [(\boldsymbol{u} \cdot \boldsymbol{\nabla})\boldsymbol{u}] = \mathrm{Pr}\,\Delta\zeta + \mathrm{Pr}\,\boldsymbol{e}_z \cdot \boldsymbol{\nabla} \times [\boldsymbol{\nabla} \cdot (\mu - 1)\dot{\boldsymbol{\gamma}}], \tag{20}$$

$$\frac{1}{\mathrm{Pr}}\left[\frac{\partial \nabla^2 w}{\partial t} - \boldsymbol{e}_z \cdot [\boldsymbol{\nabla} \times \boldsymbol{\nabla} \times [(\boldsymbol{u}.\boldsymbol{\nabla})\boldsymbol{u}]]\right] = \Delta^2 w + \mathrm{Ra}\,\nabla_H^2\theta - [\boldsymbol{\nabla} \times \boldsymbol{\nabla} \times [\boldsymbol{\nabla} \cdot (\mu - 1)\dot{\boldsymbol{\gamma}}]] \cdot \boldsymbol{e}_z, \tag{21}$$

$$\frac{\partial \theta}{\partial t} + (\boldsymbol{u} \cdot \boldsymbol{\nabla})\theta = w + \nabla^2\theta, \tag{22}$$

$$\frac{\partial \tilde{\theta}}{\partial t} = \frac{\hat{\kappa}_p}{\hat{\kappa}}\nabla^2\tilde{\theta}, \tag{23}$$

where

$$\zeta = \frac{\partial v}{\partial x} - \frac{\partial u}{\partial y} \quad \text{and} \quad \nabla_H^2 = \frac{\partial^2}{\partial x^2} + \frac{\partial^2}{\partial y^2}.$$

From the continuity equation and the vertical vorticity definition, one can deduce the horizontal velocity components $(u, v)$:

$$\nabla_H^2 u = -\frac{\partial^2 w}{\partial x \partial z} - \frac{\partial \zeta}{\partial y}; \quad \nabla_H^2 v = -\frac{\partial^2 w}{\partial y \partial z} + \frac{\partial \zeta}{\partial x}. \tag{24}$$

The boundary conditions for $w$ are

$$w = Dw = 0 \quad \text{at} \quad z = 0,1 \quad \text{for NSBC}, \tag{25}$$

and

$$w = D^2 w = 0 \quad \text{at} \quad z = 0,1 \quad \text{for SFBC}. \tag{26}$$

For the temperature, the boundary conditions are

$$\tilde{\theta} = 0 \quad \text{at} \quad z = -\Lambda, 1 + \Lambda, \tag{27}$$

$$\theta = \tilde{\theta} \quad \text{at} \quad z = 0,1, \tag{28}$$

$$D\theta = \xi\, D\tilde{\theta} \quad \text{at} \quad z = 0,1. \tag{29}$$

In the following, as in Chapman and Proctor [14], Proctor [13], and Carriere *et al.* [18], we will assume that $\hat{\kappa}_p/\hat{\kappa} = \xi$.

## III. LINER STABILITY ANALYSIS

### A. Critical conditions and critical modes

In the linear theory, $\boldsymbol{u}$ and $\theta$ are assumed infinitesimal. The nonlinear terms in (20)–(22) can be neglected. We obtain:

$$\frac{1}{\mathrm{Pr}}\frac{\partial \zeta}{\partial t} = \Delta\zeta, \tag{30}$$

$$\frac{1}{\mathrm{Pr}}\frac{\partial \Delta w}{\partial t} = \Delta^2 w + \mathrm{Ra}\Delta_H\theta, \tag{31}$$

$$\frac{\partial \theta}{\partial t} = w + \Delta\theta, \tag{32}$$

$$\frac{\partial \tilde{\theta}}{\partial t} = \frac{\hat{\kappa}_p}{\hat{\kappa}}\Delta\tilde{\theta}. \tag{33}$$

At this stage, no non-Newtonian effects enter the problem. The vertical vorticity decouples and obeys a diffusion equation and thus can be ignored in the linear theory. For Eqs. (31)–(33), we seek a normal mode solution

$$\begin{bmatrix} w(x,y,z,t) \\ \theta(x,y,z,t) \\ \tilde{\theta}(x,y,z,t) \end{bmatrix} = \begin{bmatrix} F_{11}(z) \\ G_{11}(z) \\ \tilde{G}_{11}(z) \end{bmatrix} f(x,y)\exp(s\,t), \tag{34}$$

where $s = s_r + is_i$ is a complex number and $f(x,y)$ satisfies the two-dimensional Helmoltz equation $\Delta_H f = -k^2 f$. Here $k$ is the norm of the horizontal wave number $\boldsymbol{k}$. Substituting (34) into (31)–(33) leads to the differential equations

$$s\,\mathrm{Pr}^{-1}(D^2-k^2)F_{11} = -k^2\mathrm{Ra}G_{11} + (D^2-k^2)^2F_{11}, \tag{35}$$

$$s\,G_{11} = F_{11} + (D^2-k^2)G_{11}, \tag{36}$$

$$s\,\tilde{G}_{11} = \frac{\hat{\kappa}_p}{\hat{\kappa}}(D^2-k^2)\tilde{G}_{11}. \tag{37}$$

It may be shown easily that $s$ is real. The principle of exchange of stabilities holds and hence the instability sets in a stationary convection. The boundary conditions are as follows:

$$F_{11} = DF_{11} = 0 \quad \text{at} \quad z = 0,1 \quad \text{for NSBC}, \tag{38}$$

$$F_{11} = D^2F_{11} = 0 \quad \text{at} \quad z = 0,1 \quad \text{for SFBC}, \tag{39}$$

$$\tilde{G}_{11} = 0 \quad \text{at} \quad z = -\Lambda, 1+\Lambda, \tag{40}$$

$$G_{11} = \tilde{G}_{11} \quad \text{at} \quad z = 0,1, \tag{41}$$

$$DG_{11} = \xi D\tilde{G}_{11} \quad \text{at} \quad z = 0,1. \tag{42}$$

The set of differential equations (35)–(37) is an eigenvalue problem where $s$ is the eigenvalue and $\boldsymbol{X}_{11} = (F_{11}, G_{11}, \tilde{G}_{11})$ the eigenvector. It can be written

$$s\,\boldsymbol{M}\cdot\boldsymbol{X}_{11} = \boldsymbol{L}\cdot\boldsymbol{X}_{11}. \tag{43}$$

Actually, Eq. (37) can be solved analytically:

$$\tilde{G}_{11}(z) = G_{11}(z=1)\frac{\sinh[\tilde{k}(1+\Lambda-z)]}{\sinh(\tilde{k}\Lambda)}; \quad 1 \leqslant z \leqslant 1+\Lambda, \tag{44}$$

$$\tilde{G}_{11}(z) = G_{11}(z=0)\frac{\sinh[\tilde{k}(\Lambda+z)]}{\sinh(\tilde{k}\Lambda)}; \quad -\Lambda \leqslant z \leqslant 0, \tag{45}$$

with $\tilde{k} = \sqrt{k^2 + s\hat{\kappa}/\hat{\kappa}_p}$. Hence the eigenvalue problem (35)–(37) can be restrained to the fluid domain, i.e., Eqs. (35) and (36), with the boundary conditions

$$DG_{11} = \pm\xi\tilde{k}G_{11}\coth\tilde{k}\Lambda; \quad z = 0, 1. \tag{46}$$

The eigenvalue problem (35) and (36) with the boundary conditions (46) is solved using a Chebyshev collocation method. The functions, $F_{11}$ and $G_{11}$ are expanded in series of Chebyshev polynomial series of order $N$. The $2(N+1)$ unknowns are determined at the Gauss-Lobatto nodes,

$$z_j = \frac{1}{2}\left[\cos\left(\frac{\pi\,j}{N}\right) + 1\right] \quad j = 0,1,\ldots,N. \tag{47}$$

Since $\tilde{k}$ depends on $s$, an iterative process is implemented. The eigenvector $\boldsymbol{X}_{11}$ is normalized such that

$$G_{11}(z = 1/2) = 1. \tag{48}$$

The marginal stability curve $\mathrm{Ra}(k)$ is determined by the condition $s = 0$. The minimum of the marginality stability curve gives the critical Rayleigh number $\mathrm{Ra}_c$ and $k_c$, respectively. Figure 1 displays the variation of $\mathrm{Ra}_c$ and $k_c$ as a function of the ratio $\xi$ of the thermal conductivity of the plates to that of the fluid in the case of NSBC and SFBC. The dimensionless thickness of the plates is fixed at $\Lambda = 1$. These results are in very good quantitative agreement with those obtained by Sparrow *et al.* [6], Proctor [13], Jenkins and Proctor [15], Carriere *et al.* [18], and Cerisier *et al.* [11]. The wavelength of the convection becomes larger with decreasing $\xi$ and the critical Rayleigh number $\mathrm{Ra}_c$ is also reduced.

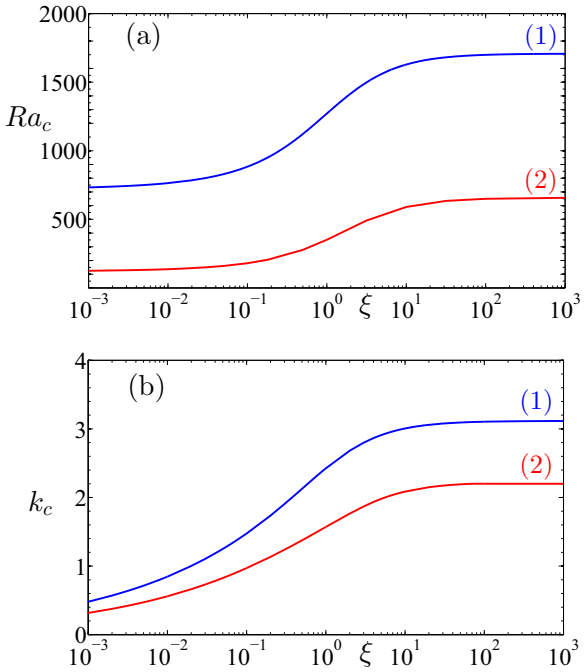


FIG. 1. (Color online) Critical Rayleigh number (a) and critical wave number (b) as a function of $\xi$ in the cases of NSBC (1) and SFBC (2).

Indeed, when a temperature fluctuation occurs in the liquid close to highly conducting wall, it easily relaxes, whereas it can persist and distorts the temperature distribution when the thermal conductivity of the boundary is very low. This temperature distortion can lead to an instability of the fluid. As a consequence, the critical Rayleigh number is smaller [11]. From mathematical point of view, the decrease of $\mathrm{Ra}_c$ is caused by the weakening of the thermal boundary conditions (28) and (29) for $\theta$ as $\xi$ decreases from $10^3$ to $10^{-3}$.

Note that for a given thermal conductivities ratio, the critical Rayleigh number for NSBC is greater than that for SFBC. The physical reason is quite intuitive. In the case of NSBC, the friction of the fluid against the wall dissipates more energy, therefore a higher thermal gradient has to be imposed so the convection can start.

When the convection flow starts, it distorts the originally horizontal isotherms. Since this deviation from the basic state occurs in the fluid layer as well as in the wall boundary, where the diffusion rate is smaller than in the fluid when $\xi < 1$, the wavelength of the convection pattern becomes larger with decreasing the thermal conductivity of the plate [19] [see Figs. 3(a) and 3(c)]. Additional properties of the critical mode are given by $F_{11}$ and $G_{11}$ at the critical conditions. They are displayed in Fig. 2 for NSBC and SFBC and different values of $\xi$. When $\xi$ decreases, the temperature perturbation does not relax at the interface, i.e., at $z = 0, 1$ [Figs. 2(c) and 2(d), curves 3, 2, and 1], thereby reducing $\mathrm{Ra}_c$. The fluctuation of the temperature gradient, $\partial\theta/\partial z$, in the liquid decreases with decreasing $\xi$ [Figs. 2(c) and 2(d)]. When $\xi \ll 1$, $\partial\theta/\partial z \to 0$, we recover the extreme situation of fixed heat flux at the boundary. Actually, for a very poor heat conductor, the horizontal scale of motion is much greater than the depth of the fluid. Therefore, vertical diffusion rates are greater than horizontal ones and the temperature perturbation becomes approximately vertically homogeneous [curve 1 in Figs. 2(c) and 2(d)]. These results are clearly illustrated by Fig. 3, where contours of the temperature perturbation are represented for three situations: (i) $\xi = 0.1$, a poor heat conductor; (ii) $\xi = 1$, $\hat{k} = \hat{k}_p$; and (iii) $\xi = 10^3$, a "perfect heat conductor." The contours shape and the convection scale at $\xi = 0.1$ [Fig. 3(a)] fundamentally differ from those at $\xi = 10^3$, a "perfect heat conductor" [Fig. 3(c)].

Figures 2(a) and 2(b) show that the vertical velocity is strongly damped with decreasing the thermal conductivity of the wall. This is a consequence of the reduction of the temperature gradient for the onset of convection as $\xi$ decreases. For the same reason, the vertical velocity is lower for SFBC than for NSBC.

### B. Characteristic time of the instability

Near the onset of convection, the growth rate Re(s) of the perturbation may be approximated using Taylor expansion of $s$ around the critical conditions:

$$s = \frac{\epsilon}{\tau_0} + O(\epsilon^2) \quad \text{with} \quad \epsilon = \frac{\mathrm{Ra} - \mathrm{Ra}_c}{\mathrm{Ra}_c}, \tag{49}$$

where $\tau_0$ is the characteristic time for the instability to grow. The determination of $\tau_0$ can be obtained either by evaluating $(\frac{ds}{d\epsilon})_{\epsilon=0}$ ($s$ is calculated for different values of $\epsilon$, around $\epsilon = 0$) or by following the methodology described by Cross [20] and

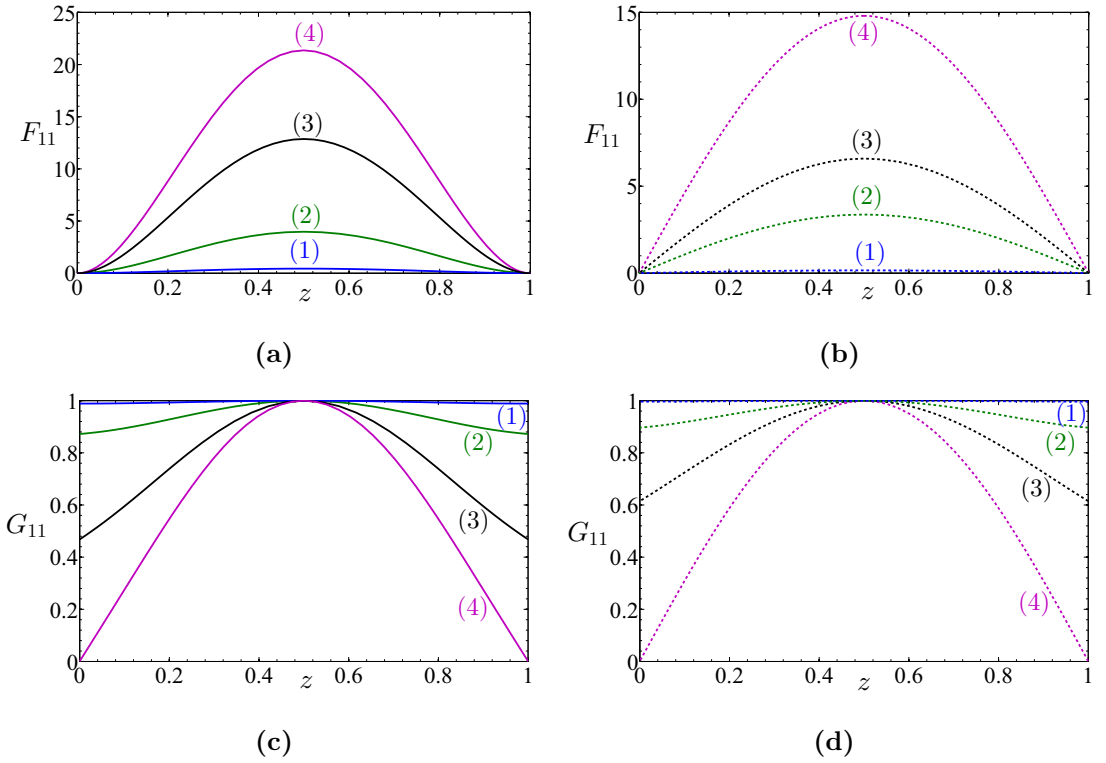


FIG. 2. (Color online) Eigenfunctions at critical conditions and different values of $\xi$: (1) $\xi = 10^{-3}$, (2) $\xi = 10^{-1}$, (3) $\xi = 10^{0}$, and (4) $\xi = 10^{3}$ in the cases of NSBC [(a)–(c)] and SFBC [(b)–(d)].

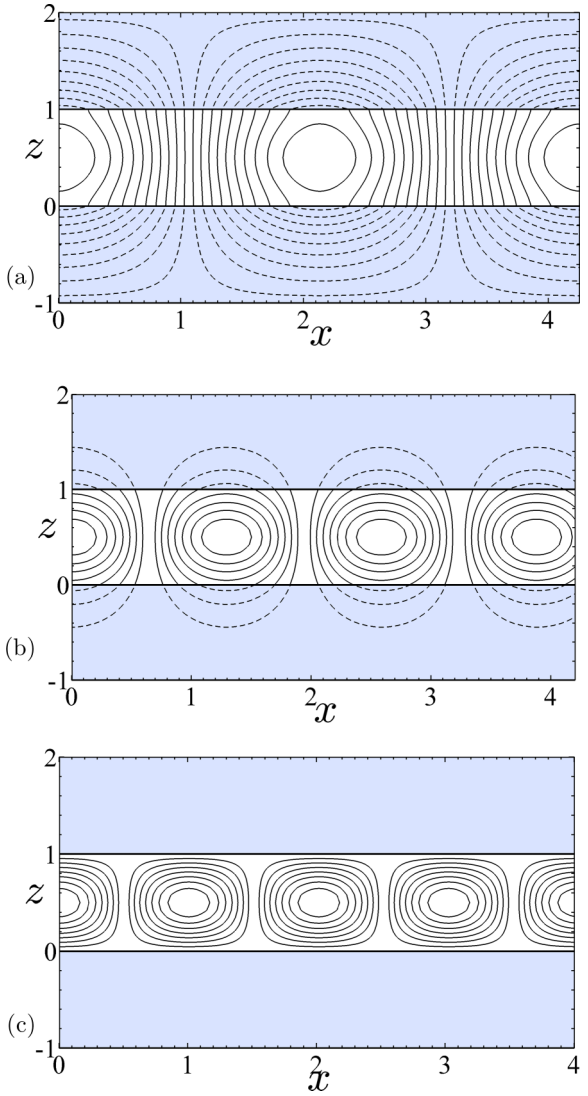


FIG. 3. (Color online) Temperature perturbation contours for three values of the thermal conductivity ratio $\xi$: (a) $\xi = 0.1$, poor heat conductor; (b) $\xi = 1, \hat{k}_p = \hat{k}$; and (c) $\xi = 1000$, "perfect heat conductor." In this latter case, the temperature perturbation in the liquid relaxes at the boundaries.

Plaut [21]. Explicitly, $\tau_0$ is given by

$$\tau_0^{-1} = \frac{-k_c^2 \mathrm{Ra}_c \langle G_{11}, F_{\mathrm{ad}} \rangle}{\langle G_{11}, G_{\mathrm{ad}} \rangle + \langle \tilde{G}_{11}, \tilde{G}_{\mathrm{ad}} \rangle + 1/\mathrm{Pr} \langle (D^2 - k^2) F_{11}, G_{\mathrm{ad}} \rangle}. \tag{50}$$

In the previous equation, $(F_{\mathrm{ad}}, G_{\mathrm{ad}})$ is the adjoint mode solution of the adjoint eigenvalue problem (Appendix A). The inner product between two functions $f$ and $g$ is defined by $\langle f, g \rangle = \int_{-\Lambda}^{1+\Lambda} f g \, dz$. The integrals are evaluated numerically by means of the Clenshaw-Curtis method in terms of the critical conditions. Note that we consider $F_{11} = G_{11} = 0$ inside the slabs and $\tilde{G}_{11} = 0$ in the fluid domain. Figure 4 shows the variation of $\tau_0$ as a function of $\xi$. As can be observed, the characteristic time of instability, $\tau_0$, varies weakly with the thermal conductivities ratio, $\xi$, when roughly $\xi > 1$. However, when $\xi < 1$, i.e., $\hat{k}_p < \hat{k}$, $\tau_0$ increases significantly

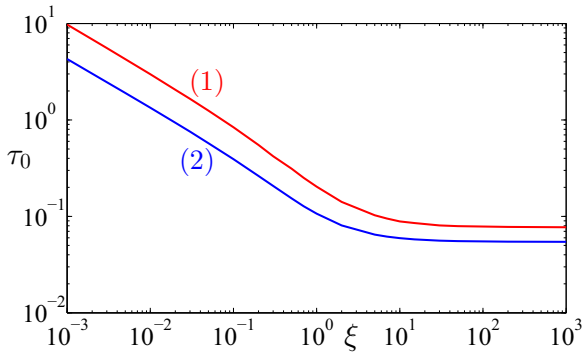


FIG. 4. (Color online) Characteristic time of instability vs thermal conductivities ratio $\xi$ at $\mathrm{Pr} = 10$. (1) SFBC and (2) NSBC.

with decreasing $\xi$ because the temperature field in the solid evolves on a more longer time with decreasing the thermal conductivity of the plates. Hence, at given $\epsilon$, the growth of the instability is slower and of longer duration as $\xi$ decreases.

## IV. WEAKLY NONLINEAR STABILITY ANALYSIS

### A. Principles and procedure

A standard weakly nonlinear convection analysis using the amplitude expansion method is adopted as a first approach to investigate nonlinear effects (see Stuart [22], Watson [23], Reynolds and Potter [24], Sen and Venkateswarlu [25], Fujimura and Yamada [26], Generalis and Fujimura [27]). At leading order, one writes

$$w(x,y,z,t) = f(x,y,t)\, F_{11}(z) + \text{c.c.}, \tag{51}$$

$$\theta(x,y,z,t) = f(x,y,t)\, G_{11}(z) + \text{c.c.}, \tag{52}$$

$$\tilde{\theta}(x,y,z,t) = f(x,y,t)\, \tilde{G}_{11}(z) + \text{c.c.} \tag{53}$$

The planform function which describes the convection pattern is

$$f(x,y,t) = \sum_{p=1}^{N} A_p(t) \exp(i\, \boldsymbol{k}_p \cdot \boldsymbol{r}), \tag{54}$$

where $|\boldsymbol{k}_p| = k_c$ and $A_p(t)$ is the amplitude of the perturbation. According to the normalization of the eigenfunctions used in the linear theory, $A_p(t)$ represents the amplitude of the thermal perturbation measured at the midplane. Configuration with $N = 1$ corresponds to rolls and $N = 2$ to squares. The weakly nonlinear analysis is applied to each of these patterns. The configuration with $N = 3$ corresponding to hexagons is not considered here. Further calculations show that this three-dimensional pattern is unstable.

In the neighborhood of the critical conditions, the dynamics are assumed to be determined by the fundamental disturbance with wave number $k = k_c$, its higher harmonics generated by the nonlinear self-interactions and the modification of the base state due to the interaction with the complex conjugate. As in Stuart [22], Watson [23], and Herbert [28], the disturbance is expanded in harmonic series and the coefficient of each harmonic is further expanded in an asymptotic series with disturbance amplitude as a small parameter.

In the case of rolls, the velocity and the temperature disturbances are expanded as follows:

$$\begin{aligned}(w(x,z;t),\theta(x,z;t),\tilde{\theta}(x,z;t)) &= \sum_{m=1}(F_{0,2m}(z),G_{0,2m}(z),\tilde{G}_{0,2m}(z))|A|^{2m} \\ &+ \sum_{n=1}\sum_{m=0}[(F_n,n+2m)(z),G_{n,n+2m})(z), \\ &\tilde{G}_{n,n+2m)}(z))|A|^{2m}A^nE^n + \text{c.c.}], \end{aligned} \tag{55}$$

where c.c. means the complex conjugate of its preceding expression, $E^n = e^{ink_cx}$, $n$ denotes the harmonic index, and $m$ indicates the asymptotic order. The time evolution of the amplitude $A(t)$ is given by the Stuart-Landau equation,

$$\frac{dA}{dt} = g_0A + g_1|A|^2A + g_2|A|^4A + \ldots. \tag{56}$$

In Eq. (56), $g_0 = s$ is the linear growth rate and $g_1$ is the first Landau constant also a first correction to the linear growth rate. The sign of $g_1$ determines whether the nature of the bifurcation is supercritical ($g_1 < 0$) or subcritical ($g_1 > 0$). If $g_1 < 0$, then the nonlinearities tend to saturate the instability, whereas if $g_1 > 0$, then a nontrivial equilibrium solution exists only if $\epsilon < 0$, but it is unstable.

Substituting expansions (55) and (56) into (21)–(23) yields after some algebra the differential equation for any $F_{n,2m+n}$, $G_{n,2m+n}$, and $\tilde{G}_{n,2m+n}$, which are solved sequentially beginning from $n = 1$ and $m = 0$.

The problem with harmonic index $n = 1$ and amplitude order $m = 0$ is the linear stability problem (35)–(37). The problem $n = 0, m = 1$ is the $O(A^2)$ correction of the conductive temperature profile due to nonlinear interactions (Appendix B). The problem $n = 2$, $m = 0$ is the first harmonic of the fundamental mode which manifests at order $O(A^2)$. The problem $n = 1, m = 1$ is the $O(A^3)$ correction to the fundamental mode. It contains nonhomogeneous terms due to nonlinear interactions. The application of the Fredholm alternative allows us to determine the first Landau constant which appears in the time derivative of $w$, $\theta$, and $\tilde{\theta}$. It can be shown that $g_1$ is the sum of contributions of two terms $g_1^I$ arising from the nonlinear inertial terms and $g_1^V$ arising from the nonlinear viscous terms. Since at the lowest order $\mu = 1 - \alpha\Gamma$, Eqs. (13) and (14), with $\alpha = \frac{1-n_c}{2}\lambda^2$, then

$$g_1 = g_1^I + g_1^V \quad \text{with} \quad g_1^V = -\alpha g_1^{NN}. \tag{57}$$

### B. Numerical method

In the above section, the nonlinear stability problem is reduced to a sequence of differential equations. As in the linear problem, they are solved using a spectral collocation method based on Chebyshev polynomials. The differential equations are collocated at Gauss-Lobatto points. The integrals involved in the determination of the first Landau constant are calculated using Clenshaw and Curtis method.

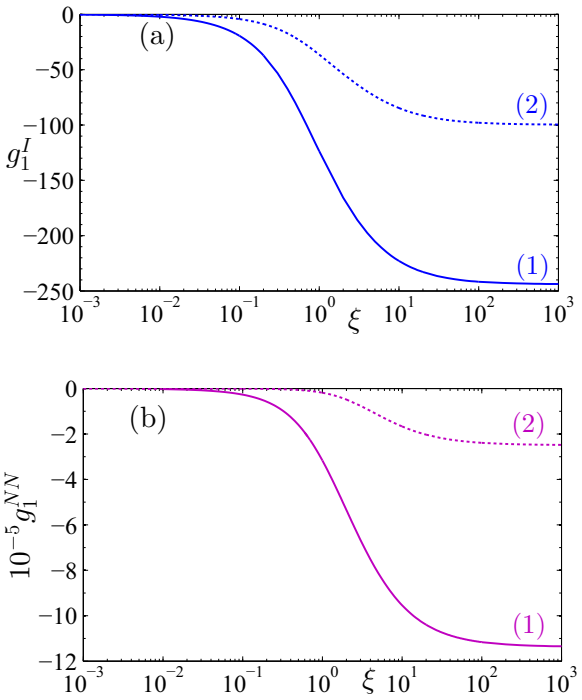


FIG. 5. (Color online) Contribution of the nonlinear inertial terms (a) and nonlinear viscous terms (b) to the first cubic Landau constant as a function of the ratio $\xi$ at Pr = 10. Curves (1) and (2) correspond to NSBC and SFBC, respectively.

## V. RESULTS AND DISCUSSION

### A. Bifurcation to rolls

The first Landau constant $g_1$ as well as the different contributions $g_1^I$ and $g_1^{NN}$ are determined for different critical sets $(\text{Ra}_c, k_c, \xi, \text{Pr})$.

In Fig. 5(a), we plot $g_1^I$ as a function of $\xi$. As expected, $g_1^I$ is negative, i.e., the bifurcation is supercritical for a Newtonian fluid. The absolute value of $g_1^I$ decreases with decreasing $\xi$ and $|g_1^I| \to 0$ when $\xi \to 0$. Note that $g_1^I$ is sensitive to change in $\xi$ mainly when $0.1 \leqslant \xi \leqslant 5$. For $\text{Pr} \geqslant 1$, the analysis of the contribution to $g_1^I$ arising from the different nonlinear interactions shows that $g_1^I$ is dominated by the nonlinear thermal convection terms involving the modification of the conductive temperature profile for all of the range of $\xi$ considered. The contribution of the nonlinear inertial term is practically negligible.

As can be observed, $g_1^{NN}$ is negative and $g_1^V = -\alpha g_1^{NN} > 0$. Therefore, shear-thinning effects promote a subcritical bifurcation, which is understandable since the viscosity, which damps convection, is reduced. In Fig. 6 we plot $g_1$ as a function of $\xi$ for different values of $\alpha$ between 0 and $5 \times 10^{-4}$. At $\xi = 10^3$, a "perfect heat conductor," the bifurcation is supercritical, $g_1 < 0$, for low shear-thinning effects and subcritical, $g_1 > 0$, for sufficiently high shear-thinning effects. At $\xi < 0.8$, the bifurcation is supercritical for the range of $\alpha$ considered. Using Eqs. (57), the critical degree of shear-thinning $\alpha_c$ above

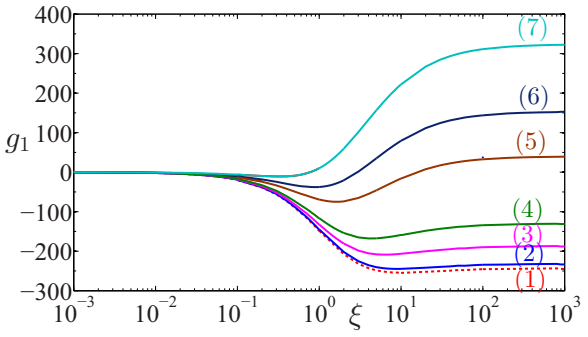


FIG. 6. (Color online) Cubic Landau constant as a function of $\xi$ in the case of NSBC with $\mathrm{Pr} = 10$ and different values of $\alpha$: (1) $\alpha = 0$, i.e., Newtonian case; (2) $\alpha = 1 \times 10^{-5}$; (3) $\alpha = 5 \times 10^{-5}$; (4) $\alpha = 10^{-4}$; (5) $\alpha = 2.5 \times 10^{-4}$; (6) $\alpha = 3.5 \times 10^{-4}$; and (7) $\alpha = 5 \times 10^{-4}$.

which the bifurcation changes from supercritical to subcritical is given by

$$\alpha_c = \frac{g_1^I}{g_1^{NN}}. \tag{58}$$

Figure 7 shows the variation of $\alpha_c$ as a function of $\xi$ at $\mathrm{Pr} = 10$ for NSBC and SFBC. The more $\xi$ is low, the more the degree of shear thinning $\alpha$ of the fluid must be high to obtain a subcritical bifurcation. It must be even higher in the case of SFBC than in NSBC. These results are related to the reduction of the convection intensity when $\xi$ decreases as shown by Figs. 2(a) and 2(b) and therefore to a lower modification of the viscosity. Note that the largest variation of $\alpha_c$ with $\xi$ occurs mainly for $10^{-2} \leqslant \xi \leqslant 10$.

### B. Bifurcation to squares

For square patterns, considered as the superposition of two perpendicular sets of rolls, the amplitude equations are [29]

$$\frac{dA_1}{dt} = s\,A_1 + \left[g_1 A_1^2 + \lambda_1 A_2^2\right]A_1, \tag{59}$$

$$\frac{dA_2}{dt} = s\,A_2 + \left[g_1 A_2^2 + \lambda_1 A_1^2\right]A_2. \tag{60}$$

As for $g_1$, the coefficient of cross saturation $\lambda_1$ is obtained by invoking the solvability condition and can be written as:

$$\lambda_1 = \lambda_1^I - \alpha\lambda_1^{NN}. \tag{61}$$

The numerical results indicate that $\lambda_1^I$ and $\lambda_1^{NN}$ are negative and their variation with $\xi$ is similar to that of $g_1^I$ and $g_1^{NN}$, respectively. The critical value of $\alpha$ above which, the bifurcation becomes subcritical is given by

$$\alpha_c = \frac{g_1^I + \lambda_1^I}{\left(g_1^{NN} + \lambda_1^{NN}\right)}. \tag{62}$$

The variation of $\alpha_c$ as a function of $\xi$, at $\mathrm{Pr} = 10$, is depicted in Fig. 8 for NSBC and SFBC. As in the case of rolls, $\alpha_c$ increases with decreasing $\xi$.

The influence of Prandtl number on $\alpha_c$ is shown in Fig. 9 for two limit values of $\xi$: $10^{-3}$ and $10^3$. At $\xi = 10^3$ ("perfect heat conductor"), the occurrence of subcritical convection is practically independent of Pr when $\mathrm{Pr} \geqslant 10$. The nonlinear inertial terms ($[(\boldsymbol{u}\cdot\nabla)\boldsymbol{u}$ term] in Eq. (5) which in dimensionless

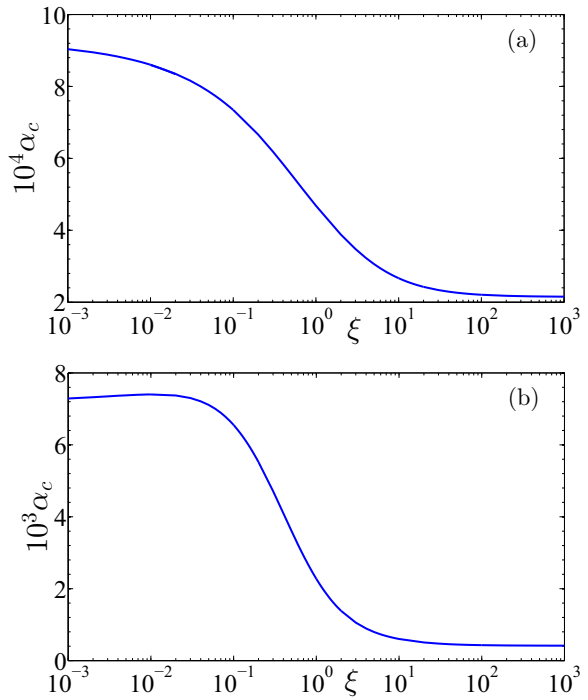


FIG. 7. (Color online) For rolls, critical value of the degree of shear-thinning $\alpha_c$ vs the thermal-conductivities ratio $\xi$ at $\mathrm{Pr} = 10$ for (a) NSBC and (b) SFBC.

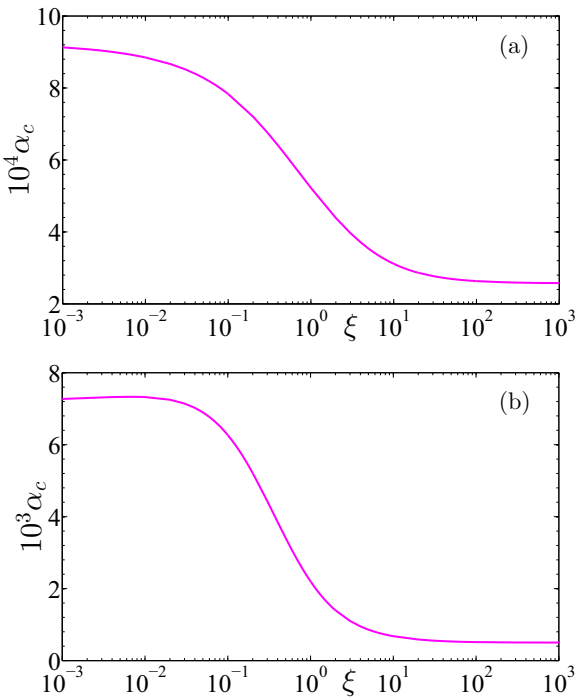


FIG. 8. (Color online) For squares, critical value of the degree of shear-thinning $\alpha_c$ vs the thermal-conductivities ratio $\xi$ at $\mathrm{Pr} = 10$ for (a) NSBC and (b) SFBC.

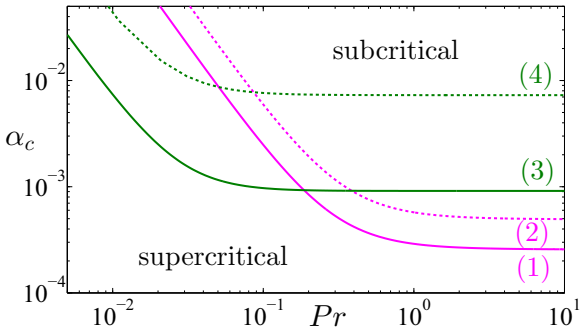


FIG. 9. (Color online) Critical value of the degree of shear-thinning $\alpha_c = (|\frac{d\mu}{dT}|_{\Gamma=0})_c$ as a function of Prandtl number. Case of square patterns. (1) NSBC with $\xi = 10^3$; (2) SFBC with $\xi = 10^3$; (3) NSBC with $\xi = 10^{-3}$; (4) SFBC with $\xi = 10^{-3}$.

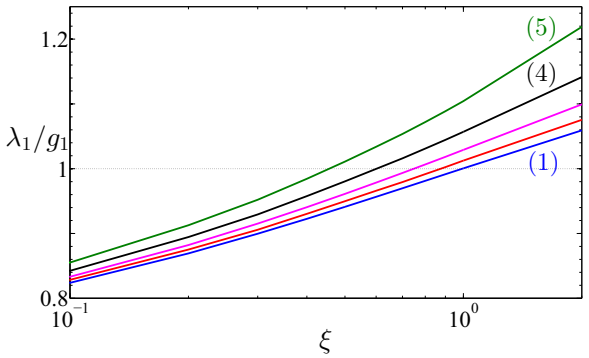


FIG. 10. (Color online) Ratio of the cross saturation coefficient $\lambda_1$ to the saturation coefficient $g_1$ versus the ratio of the thermal conductivities $\xi$ for different values of the shear-thinning degree $\alpha$ in the case of NSBC. (1) $\alpha = 0$; (2) $\alpha = 2.5 \times 10^{-5}$; (3) $\alpha = 5.625 \times 10^{-5}$; (4) $\alpha = 10^{-4}$; (5) $\alpha = 1.5625 \times 10^{-4}$.

units are multiplied by $\mathrm{Pr}^{-1}$ have no influence from $\mathrm{Pr} = 10$, whereas at $\xi = 10^{-3}$ (very poor heat conductor), the nonlinear inertial terms play practically no role from $\mathrm{Pr} \approx 0.1$, this is not surprising since the intensity of convection is strongly damped when $\xi \ll 1$.

At low Prandtl number, say, $\mathrm{Pr} < 0.05$, $\alpha_c$ increases strongly with decreasing Pr.

### C. Pattern selection

In this section, we investigate the pattern selection on a square lattice. The calculation proceeds in two stages. First, the possible steady-state solutions of the amplitude equations are determined. Then their linearized stability is determined by computing the eigenvalues of the linearized system around each solution. A solution is stable if all its eigenvalues are negative.

The system of amplitude equations for a square lattice are given by Eqs. (59) and (60). The coefficients $s$, $g_1$, and $\lambda_1$ in these equations depend on the rheological parameters and on the reduced Rayleigh number $\epsilon = (\mathrm{Ra} - \mathrm{Ra}_c)/\mathrm{Ra}_c$. The stationary solutions are obtained by setting $f_i(A_1, A_2) = 0$, where $f_i$ is the right-hand side of the amplitude equations. Their stability is determined by the sign of the eigenvalues $\chi_i$ of the Jacobian matrix $\boldsymbol{J}_{ij} = \frac{\partial f_i}{\partial A_j}$ evaluated at the steady states. In the following, the stability of the stationary solutions is examined in details.

(i) Conduction state, $A_1 = A_2 = 0$. The eigenvalues associated to this state are $\chi_1 = \chi_2 = s$. The conduction state is stable if $\epsilon < 0$ and undergoes a stationary bifurcation at $\epsilon = 0$.

(ii) Steady convection with rolls parallel to $\boldsymbol{e}_x$ or $\boldsymbol{e}_y$, $A_1 = \sqrt{-s/g_1}$, $A_2 = 0$, or $A_1 = 0$, $A_2 = \sqrt{-s/g_1}$. The eigenvalues associated to this state are $\chi_1 = -2s$ and $\chi_2 = s\frac{g_1 - \lambda_1}{g_1}$.

(iii) Steady convection with square patterns, $A_1 = A_2 = \sqrt{-s/(g_1 + \lambda_1)}$. The eigenvalues associated to this steady state are $\chi_1 = -2s$ and $\chi_2 = \frac{2s(\lambda_1 - g_1)}{\lambda_1 + g_1}$.

In the supercritical regime, i.e., $s > 0$ and $\chi_1 < 0$. The sign of $\chi_2$ depends on the ratio $\lambda_1/g_1$. It is represented in Fig. 10 as a function of $\xi$ for different values of $\alpha$. When $|\lambda_1| > |g_1|$, $\chi_2$ is positive and the squares are unstable. According to Ref. [30], the interaction between the two sets of rolls is too strong and one of the two sets of rolls nonlinearly damps out the other. When $|\lambda_1| < |g_1|$, $\chi_2 < 0$ and the squares are stable. The critical value of $\xi$ at which the planform of convection changes from square-cell solution ($\xi < \xi_c$) to two-dimensional roll solution ($\xi > \xi_c$) is given as a function of $\alpha$ in Fig. 11. In the Newtonian case, i.e., $\alpha = 0$, $\xi_c = 1$. This result is in agreement with that given by Jenkins and Proctor [15]. With increasing shear thinning effects, the interaction between the two sets of rolls of a square-cell increases, reducing by this way, $\xi_c$.

## VI. SOLUTIONS AT HIGHER ORDER

Figure 11 is obtained by truncating the series (56) to the first Landau constant, i.e., at cubic order in $A$. For a significant deviation from the critical conditions, terms of higher order become large and should be taken into account. A weakly nonlinear expansion was then carried out up to fifth-order in amplitude. Figure 12 shows the evolution of $\xi_c$ versus the reduced Rayleigh number, $\epsilon$, for different values of the constant time of the fluid $\lambda$. The shear-thinning index is fixed to $n = 0.5$. The intensity of convection increases with increasing $\epsilon$. The interaction between the two sets of rolls via nonlinear inertial and nonlinear viscous terms become stronger leading to a diminution of $\xi_c$.

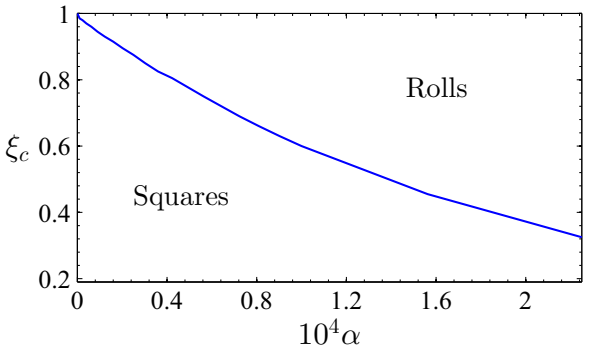


FIG. 11. (Color online) $\xi_c$ as a function of $\alpha$ for NSBC with $\mathrm{Pr} = 10$ and $\Lambda = 1$. The planform of convection is a square cell when $\xi < \xi_c$ and a two-dimensional roll when $\xi > \xi_c$.

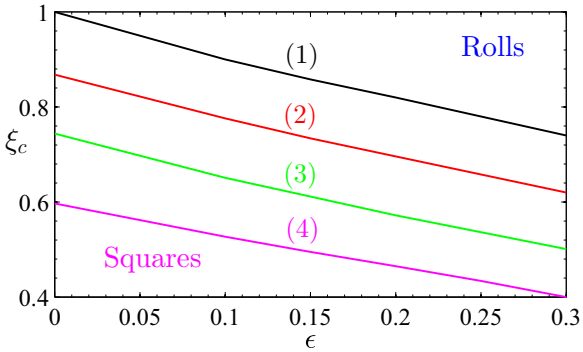


FIG. 12. (Color online) $\xi_c$ as a function of $\epsilon$ for NSBC with $n_c = 0.5$, Pr $= 10$, and $\Lambda = 1$. Squares are stable for $\xi < \xi_c$, and rolls are stable for $\xi > \xi_c$. (1) $\lambda = 0$, (2) $\lambda = 0.01$, (3) $\lambda = 0.015$, (4) $\lambda = 0.02$.

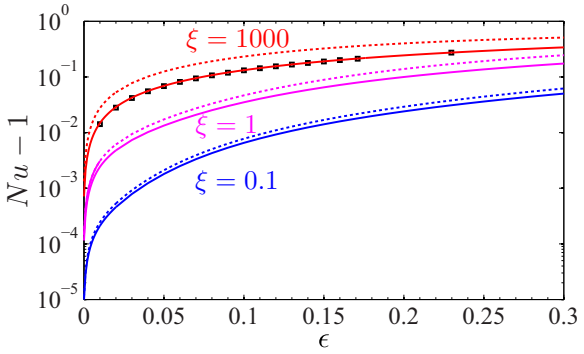


FIG. 13. (Color online) Nusselt number as a function of the reduced Rayleigh number $\epsilon$ in the case of NSBC at Pr $= 10$ and for three values of $\xi$. The continuous lines correspond to a Newtonian fluid and the dashed lines to a shear-thinning fluid with $n = 0.5$, $\lambda = 0.02$; (□) numerical solution of (21) and (22) obtained using the spectral code of Plaut and Busse [31] in the case of a Newtonian fluid with perfectly conducting walls.

## VII. HEAT TRANSFER, FLOW STRUCTURE, AND VISCOSITY FIELD

In the present section, information on the heat transfer, the flow structure, and the viscosity field in rolls and squares are provided. The influence of shear thinning will be emphasized.

### A. Heat transfer

The heat transfer through the horizontal fluid layer is described by the Nusselt number, Nu, the ratio of the total heat flux to the purely conductive heat flux in the absence of fluid flow. It can be calculated either at the lower or upper plate. At the lower plate, we have

$$\mathrm{Nu} = 1 - \left(\frac{\partial \bar{\theta}}{\partial z}\right)_{z=0} = 1 - \sum_{p=1}^{N}\sum_{m=1}^{M}\left[A_p^{2m}(DG_{02m})_{z=0}\right] - S\,A_1^2 A_2^2 (D\underline{G}_{04})_{z=0}, \tag{63}$$

where the overbar denotes the horizontal average over one wavelength, $N = 1$ corresponds to rolls and $N = 2$ to squares, $M = 1$ when the series (56) is truncated at the third order and $M = 2$ when (56) is truncated at the fifth order, $S = 1$ for squares, and $S = 0$ for rolls. The term $D\underline{G}_{04}$ arises from the interaction between modes with different eigenvectors. The unperturbed solution, Nu $= 1$, corresponds to the hydrostatic solution. The second term of Nu refers to the convective transfer.

Figure 13 shows for a two-dimensional roll solution computed at the fifth order the evolution of Nu $- 1$ as a function of $\epsilon$ for different values of $\xi$. The Nusselt number decreases with decreasing $\xi$ because of the decrease of the perturbation heat flux at the boundaries. This is illustrated, for instance, by Fig. 16 in Appendix B, where $(dG_{0,2}/dz)$ at $z = 0,1$ decreases with decreasing $\xi$. When $\xi \to 0$, i.e., for poorly conducting plates, we recover the situation of fixed heat flux, the temperature gradient does not fluctuate, $\partial\theta/\partial z = 0$, and Nu $\to 1$. The convection in the fluid layer will not contribute to the overall heat transfer. For $\xi = 1000$, to represent the case of perfectly conducting walls, our results are in good agreement with the numerical solution of (21) and (22) obtained using the spectral code of Ref. [31], at least up to $\epsilon = 0.25$. The influence of shear-thinning effects is illustrated by the dotted curves. The Nusselt number increases with increasing shear-thinning effects (Pierre and Tien [32], Liang and Acrivos [33], Ozoe and Churchill [34], Lamsaadi *et al.* [35], Aloui *et al.* [36], Bouteraa *et al.* [1]). For low values of $\xi$, the influence of shear-thinning effects is reduced. Figure 14 shows Nu $- 1$ as a function of $\epsilon$ for rolls and squares at two values of $\xi$: 0.1 and 1. At $\xi = 0.1$, the Nusselt number is larger for squares than for rolls, while at $\xi = 1$, Nu is greater for rolls than for squares. The differences are small but notable and in

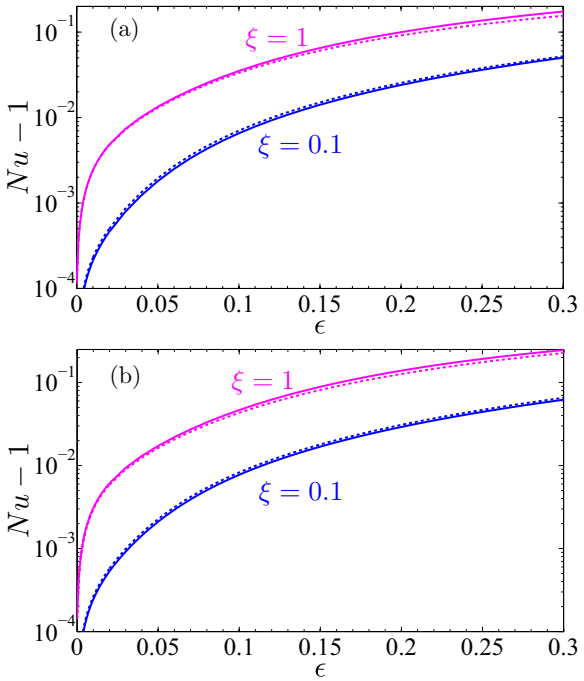


FIG. 14. (Color online) Nusselt number as a function of the reduced Rayleigh number $\epsilon$ in the case of NSBC with Pr $= 10$ and for two values of $\xi$. (a) Newtonian fluid and (b) shear-thinning fluid with $n = 0.5$ and $\lambda = 0.02$. The continuous lines correspond to rolls and the dashed lines to squares.

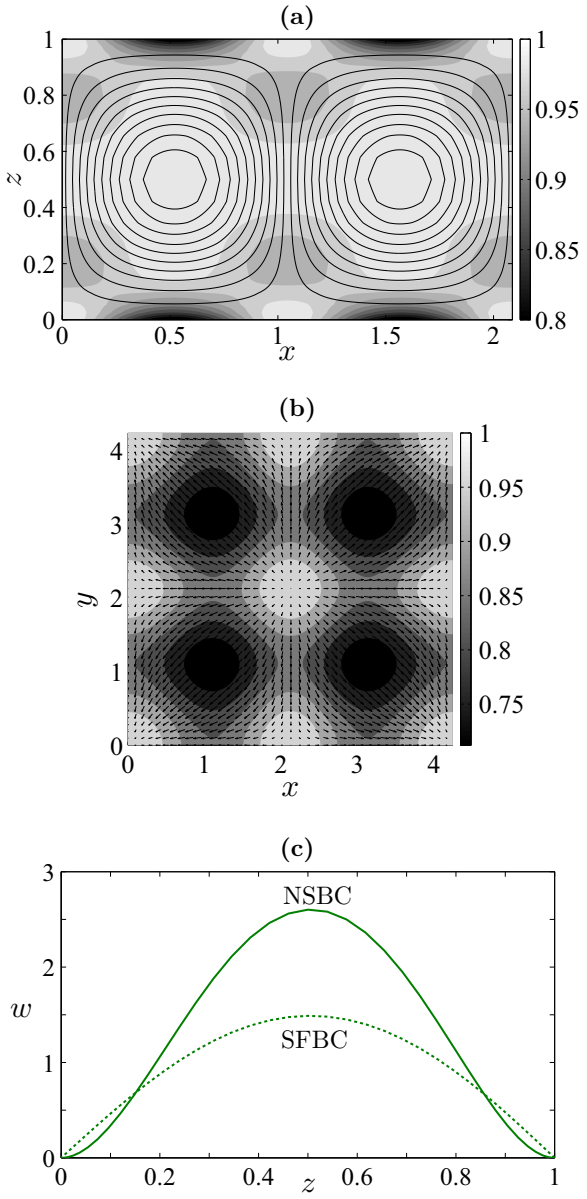


FIG. 15. (Color online) Flow structure and viscosity distribution over a roll [(a) $\xi = 1000$] and a square [(b) $\xi = 0.1$] at $\epsilon = 0.2$, with NSBC, $\alpha = 0.2\alpha_c$ and Pr $= 10$. For the square, the horizontal velocity field is shown at $z = 0.8$. (c) Vertical velocity profile in the square cell center for NSBC and SFBC.

agreement with the maximum heat transfer principle: The only stable solution is the one of maximum heat transport (Malkus and Veronis [37]).

### B. Viscosity field

The viscosity distribution for rolls and square cells, computed at the fifth order in amplitude, is shown in Fig. 15 for $\epsilon = 0.2$. Two values of $\xi$ are considered. The first one is $\xi = 1000$, where rolls are stable, and the second one is $\xi = 0.1$, where squares are stable. For the rheological parameters, we set $n$ and $\lambda$ such that $\alpha = 0.2\alpha_c$.

#### 1. *Rolls:* $\xi = 1000$ *with NSBC*

The viscosity field and the flow structure are illustrated by Fig. 15(a). The interior of the roll is practically isoviscous with $\mu \approx 1$. The viscosity is minimal at the wall where the shear rate is maximal. It is weakly reduced at the four corners of the roll because of the elongational rate $\dot{\gamma}_{zz} = -\dot{\gamma}_{xx}$.

#### 2. *Squares:* $\xi = 0.1$ *with NSBC*

Because of the symmetry of the solution, considered as a superposition of two equal-strength perpendicular roll sets in the $x$ and $y$ directions, no fluid passes through the vertical diagonal planes and the vertical cell boundaries. Since the amplitude equations on a square lattice involve $A$ in the form of $A^2$, there are two equiprobable opposite motions (as for rolls). In the first one, the fluid is downwardly directed in the cell center and upwardly through the vertical cell boundaries. In the second one, the fluid is upwardly directed in the cell center and downwardly through the vertical cell boundaries. We have chosen to represent the second case. The vertical velocity profile is shown in Fig. 15(c) for NSBC ans SFBC. The viscosity field and the flow structure are displayed in Fig. 15(b). At the wall and around the stagnation points (light region in the figure), the viscosity is weakly reduced. The viscosity is minimal at locations (dark region in the figure) where the shear rates $\dot{\gamma}_{xz}$ and $\dot{\gamma}_{yz}$ are maximal.

## VIII. CONCLUSION

We have investigated the influence of shear-thinning effects on the convection in a horizontal layer of a shear-thinning fluid between two horizontal symmetric plates of finite thermal conductivity. The rheological behavior of the fluid is described by the Carreau model. The critical Rayleigh number $\mathrm{Ra}_c$ and wave number $k_c$ for the onset of convection are determined as a function of the ratio $\xi$ of the thermal conductivity of the plates to that of the fluid. As the fluid viscosity at zero shear rate is constant, the values of $\mathrm{Ra}_c$ and $k_c$ in NSBC and SFBC are in very good quantitative agreement with those given in the literature for a Newtonian fluid. Additional results dealing with the characteristic time of instability $\tau_0$ are provided. It is found that $\tau_0$ increases significantly when $\xi < 1$, and the growth of the instability is slower and of longer duration. The nature of the bifurcation to rolls and squares has been determined using a three-dimensional weakly nonlinear approach of amplitude equations. The critical value of the shear-thinning degree $\alpha_c$ above which the bifurcation becomes subcritical is determined as a function of $\xi$. It is shown that $\alpha_c$ increases with decreasing $\xi$ due to the reduction of the convection intensity. For the same reason, the limit value of Prandtl number from which the nonlinear inertial $[(\boldsymbol{u}\cdot\boldsymbol{u})\boldsymbol{u}]$ terms of inertia can be neglected varies from 10 for a "perfect heat conductor" to 0.1 for a very poor heat conductor. The stability of rolls and squares is then investigated as a function of $\xi$ and the rheological parameters. In the Newtonian case, squares are stable when $\xi < 1$, in agreement with Ref. [15]. In the case of shear-thinning fluids, an additional nonlinear coupling between modes is introduced by the rheological law. This leads to a decrease of the critical value of $\xi$ below which squares are stable.

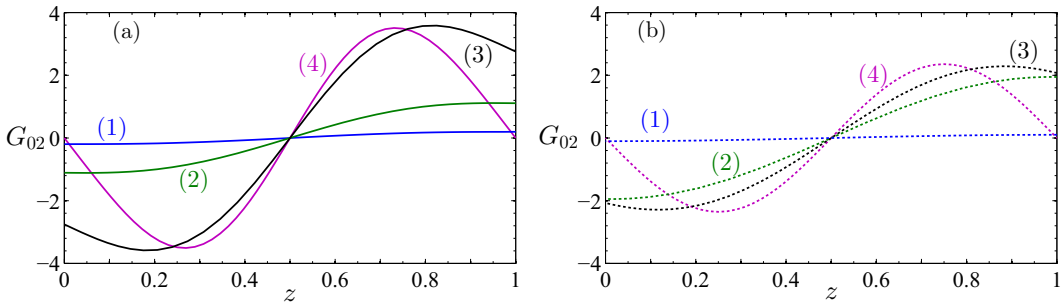


FIG. 16. (Color online) Modification of the conductive temperature profile at the critical conditions for Pr = 10 and different values of $\xi$: (1) $\xi = 10^{-3}$; (2) $\xi = 10^{-1}$; (3) $\xi = 10^{0}$; and (4) $\xi = 10^{3}$ in the case of NSBC (a) and SFBC (b).

By considering the amplitude expansion at the fifth order, the range of validity of the weakly nonlinear analysis is extended and the domain of stability of the square pattern in the $(\xi,\epsilon)$ plane is determined. These results are consistent with the maximum heat-transfer principle.

In the weakly nonlinear approach, it is assumed implicitly that the dynamics is dominated by the fundamental mode. We intend to analyze the stability of the convective patterns, in the space Rayleigh wave number, as a function of $\xi$ and shear-thinning effects.

## ACKNOWLEDGMENTS

The authors gratefully acknowledge the financial support of the French National Research Agency under Grant No. ANR-10-BLAN-925-01.

## APPENDIX A: ADJOINT MODE

First, we need to define an inner product between two vectors $\boldsymbol{f}$ and $\boldsymbol{g}$ by

$$\langle \boldsymbol{f},\boldsymbol{g}\rangle = \int_{-\Lambda}^{1+\Lambda} \boldsymbol{f}\cdot\boldsymbol{g}\,dz. \tag{A1}$$

The adjoint mode $\boldsymbol{X}_{\rm ad}$ associated to the critical mode $\boldsymbol{X}_{11}$ verifies the adjoint eigenvalue problem,

$$\boldsymbol{L}^{+}\cdot\boldsymbol{X}_{\rm ad} = 0. \tag{A2}$$

The adjoint operator $\boldsymbol{L}^{+}$ of operator $\boldsymbol{L}$ is defined by

$$\langle \boldsymbol{X}_{\rm ad},\boldsymbol{L}\cdot\boldsymbol{X}\rangle = \langle \boldsymbol{L}^{+}\cdot\boldsymbol{X}_{\rm ad},\boldsymbol{X}\rangle. \tag{A3}$$

## APPENDIX B: MODIFICATION OF THE CONDUCTIVE TEMPERATURE PROFILE AT ORDER $A^2$

The correction of the conductive temperature profile in the fluid at order $A^2$ satisfies the following equation:

$$(D^2-2s)G_{02} = 2[G_{11}(DF_{11}) + F_{11}(DG_{11})] \tag{B1}$$

with

$$DG_{02} = \pm\xi G_{02}; \quad \text{at} \quad z = 0,1. \tag{B2}$$

Figure 16 shows the modification of the conductive temperature profile at order $A^2$ in NSBC and SFBC. It is noteworthy that $dG_{02}/dz$, at $z = 0,1$, decreases with decreasing $\xi$ and $dG_{02}/dz \to 0$ for a very poor heat conductor.

[1] M. Bouteraa, C. Nouar, E. Plaut, C. Métivier, and A. Kalck, J. Fluid Mech. **767**, 696 (2015).
[2] P. LeGal and V. Croquette, Phys. Fluids **31**(11), 3440 (1988).
[3] A. Gorius, B. Perrin, and S. Fauve, J. Phys. Lett. **46**, 295 (1985).
[4] Z. Kebiche, Etude expérimentale de l'instabilité de Rayleigh-Bénard dans les fluides non-Newtoniens, Ph.D. thesis, Université de Nantes, 2014.
[5] Z. Kebiche, C. Castelain, and T. Burghelea, J. Non-Newtonian Fluid Mech. **203**, 9 (2014).
[6] E. Sparrow, R. Goldstein, and V. Jonsson, J. Fluid Mech. **18**, 513 (1964).
[7] D. T. J. Hurle, E. Jakeman, and E. R. Pike, Proc. R. Soc. Lond. A **296**, 469 (1967).
[8] N. Riahi, J. Fluid Mech. **129**, 153 (1983).
[9] R. M. Clever and F. H. Busse, Phys. Rev. E **57**, 4198 (1998).
[10] B. Holmedal, M. Tveitereid, and E. Palm, J. Fluid Mech. **537**, 255 (2005).
[11] P. Cerisier, S. Rahal, J. Cordonnier, and G. Lebon, Int. J. Heat Mass Transf. **41**, 3309 (1998).
[12] F. H. Busse and N. Riahi, J. Fluid Mech. **96**, 243 (1980).
[13] R. Proctor, J. Fluid Mech. **113**, 469 (1981).
[14] C. J. Chapman and M. R. E. Proctor, J. Fluid Mech. **101**, 759 (1980).
[15] D. R. Jenkins and M. R. E. Proctor, J. Fluid Mech. **139**, 461 (1984).
[16] R. B. Bird, R. Amstrong, and O. Hassager, *Dynamics of Polymeric Liquids* (Wiley-Interscience, New York, 1987).
[17] R. Tanner, *Engineering Rheology* (Oxford University Press, New York, 2000).
[18] P. Carriere, A. Bottaro, and P. Metzener, Eur. J. Mech. B/Fluids **16**, 483 (1997).
[19] M. Westerburg and F. H. Busse, J. Fluid Mech. **432**, 351 (2001).
[20] M. Cross, Phys. Fluids **23**(9), 1727 (1980).
[21] E. Plaut, Modélisation d'instabilités par méthodes nonlinéaires, Master course, Université de Lorraine, 2008.
[22] J. T. Stuart, J. Fluid Mech. **9**, 353 (1960).
[23] J. Watson, J. Fluid Mech. **9**, 371 (1960).
[24] W. C. Reynolds and M. C. Potter, J. Fluid Mech. **27**, 465 (1967).

[25] P. Sen and D. Venkateswarlu, J. Fluid Mech. **133**, 179 (1983).
[26] K. Fujimura and S. Yamada, Proc. R. Soc. Lond. A **464**, 2721 (2008).
[27] S. Generalis and K. Fujimura, J. Phys. Soc. Jpn. **78**, 1 (2009).
[28] T. Herbert, J. Fluid Mech. **126**, 167 (1983).
[29] M. Golubitsky, J. Swift, and E. Knoblock, Physica D **10**, 249 (1984).
[30] S. Fauve, Pattern forming instabilities, in *Hydrodynamics and Nonlinear Instabilities*, edited by P. Huerre and M. Rossi (Cambridge University Press, Cambridge, 1998).
[31] E. Plaut and F. H. Busse, J. Fluid Mech. **464**, 345 (2002).
[32] S. C. Pierre and C. Tien, Can. J. Chem. Eng. **41**, 122 (1963).
[33] S. F. Liang and A. Acrivos, Rheol. Acta **9**, 447 (1970).
[34] H. Ozoe and S. W. Churchill, AIChE Symp. Ser. **69**, 126 (1973).
[35] M. Lamsaadi, M. Naimi, and M. Hasnaoui, Heat Mass Transfer **41**, 239 (2005).
[36] Z. Alloui, N. B. Khelifa, H. Beji, P. Vasseur, and A. Guizani, J. Non-Newtonian Fluid Mech. **196**, 70 (2013).
[37] W. V. R. Malkus and G. Veronis, J. Fluid Mech. **4**, 225 (1958).